Eur. Phys. J. C manuscript No.
(will be inserted by the editor)

Physics potential for the H→ZZ decay at the CEPC

Ryuta Kiuchi[1], Yanxi Gu[2], Min Zhong[2], Lingteng Kong[3], Alex Schuy[4], Shih-Chieh Hsu[b,4], Xin Shi[a,1], Kaili Zhang[1]

[1]Institude of High Energy Physics, Chinese Academy of Science, Beijing 100049, China
[2]Department of Modern Physics, University of Science and Technology of China, Hefei 230026, China
[3]University of Chinese Academy of Sciences, Beijing, 100049, China
[4]Department of Physics, University of Washington, Seattle 98195-1560, USA

Received: date / Accepted: date

Abstract The precision of the yield measurement of the Higgs boson decaying into two Z bosons process at the Circular Electron-Positron Collider (CEPC) is evaluated. Including the recoil Z boson associated with the Higgs production (Higgsstrahlung) total three Z bosons are produced for this channel, from which final states characterized by the presence of a pair of leptons, quarks, and neutrinos are chosen for the signal. Two analysis approches are compared and the final precision of σ_{ZH}·Br(H→ZZ) is estimated to be 7.89% using a multivariate analysis technique, based on boosted decision trees. The relative precision of the Higgs boson width, using this H→ZZ decay topology, is estimated by combining the obtained result with the precision of the inclusive ZH cross section.

Keywords CEPC · Higgs boson · Higgs to ZZ

1 Introduction

After the discovery of the Higgs boson [1,2], efforts are performed on measuring properties of the Higgs boson. One of motivations of these studies is to obtain hints for physics beyond the Standard Model (SM), whose existence is suggested by several experiment facts, such as dark matter, cosmological baryon-antibaryon asymmetry. The Circular Electron-Positron Collider (CEPC) [3, 4] is a proposed future circular e^+e^- collider, having its main ring circumstance of ∼100 km. As a Higgs factory, the CEPC is planned to operate at $\sqrt{s} = 240$ GeV with on integrated luminosity of 5.6 ab^{-1} which is expected to achieve an order of magnitude improvement on measurements of Higgs boson properties as compared to the final LHC precision.

[a]e-mail: shixin@ihep.ac.cn
[b]e-mail: schsu@uw.edu

The Higgs production mechanisms at $\sqrt{s} = 240$ GeV will be the Higgsstrahlung process e^+e^-→Z*→ZH (hereafter, denoted as ZH process) and the vector boson fusion processes, e^+e^-→W^{+*}W$^{-*}\nu_e\bar{\nu}_e$→H$\nu_e\bar{\nu}_e$ ($\nu\bar{\nu}$H process) and e^+e^-→Z*Z*e^+e^-→He^+e^-. Among these processes, the Higgsstrahlung process is dominating over all of the others. Therefore, it is going to provide series of the Higgs measurements, such as the cross section $\sigma(ZH)$, using the recoil mass method against the Z boson. That Z boson also serves as a tag of the ZH process by identifying decay fermions from it. With this tag information, individual decay channels of the Higgs boson will be explored subsequently and give us valuable information on the Higgs boson properties.

The Higgs decay into a pair of Z bosons, via the ZH process, will be studied at the CEPC. Like the other decay modes, the Branching ratio BR(H→ZZ) can be obtained from the measurement of the signal yield, $\sigma(ZH)$×BR(H→ZZ). In addition, the Higgs boson width $\Gamma_{\rm H}$ can be inferred as well. Under the assumption that the coupling structure follows the SM, the branching ratio is proportional to BR(H→ZZ) = Γ(H→ZZ)/$\Gamma_{\rm H}$ ∝ $g^2_{\rm HZZ}/\Gamma_{\rm H}$, therefore, $\Gamma_{\rm H}$ is deduced with the uncertainty from the measurement of the coupling $g^2_{\rm HZZ}$ (σ(ZH)∝$g^2_{\rm HZZ}$) and the signal yield. Note that the vector boson fusion $\nu\bar{\nu}$H process in combination with measurements of final states from H→WW decay will also contribute to the $\Gamma_{\rm H}$ value and consequently the final value will be determined from the combination of the two measurements[4,5].

The study of H→ZZ channel via the ZH process has an unique feature among the other decays that is originated from its event topology where two on-shell Z bosons and one off-shell Z boson are involved. Considering various Z boson's decay possibilities, the topology diverges into lots of final states. H→ZZ→4l decay

is the so-called "golden channel" of the Higgs boson study at the LHC, as it has the cleanest signature of all the possible Higgs boson decay modes. However, the statistics of this leptonic channel at the CEPC may not allow to study the properties with required precision. Conversely, fully hadronic channel can provide enough statistics, but difficulties in identifying and matching jets with proper Z bosons, as well as efficient separation from the SM backgrounds have to be overcome. Between these two extremes, the decay channels having a pair of leptons, two jets and two neutrinos are most promising candidates for studying H→ZZ properties, owing to its clear signature and larger branching fraction than the leptonic channel. Therefore, this final state has been chosen as the signal for the evaluation of the H→ZZ properties. Muons have most advantage among charged leptons for discriminating isolated status from those produced by semi-leptonic decays of heavy flavor jets and the final states including a pair of muons are selected as the signal process: $Z\to\mu^+\mu^-$, $H\to ZZ^*\to\nu\bar{\nu}q\bar{q}$ (Fig. 1) and its cyclic permutations, $Z\to\nu\bar{\nu}$, $H\to ZZ^*\to q\bar{q}\mu^+\mu^-$ and $Z\to q\bar{q}$, $H\to ZZ^*\to\mu^+\mu^-\nu\bar{\nu}$, where the q represents all quark flavors except for the top quark. On the other hand, various final states involved in this analysis can serve as validation for detector reconstruction on charged particles. It puts anc overall test on whether the design and detector calibration precision has reached our demand.

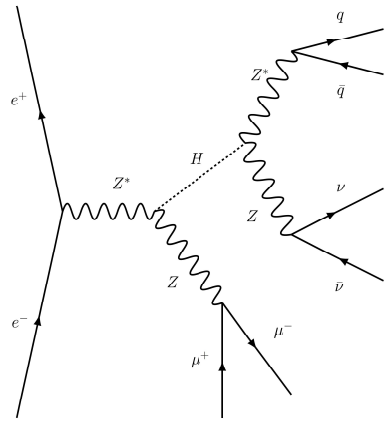

Fig. 1 Example Feynman diagram of the signal process which is characterized by the presence of a pair of muons, jets and neutrinos. In this example, the initial Z boson associated with the Higgs production is decaying into muons whereas cyclic permutation of the decay products from 3 Z bosons is considered in the analysis.

In this article, we report on the estimation of relative accuracy of the yield measurement for the H→ZZ decay at the CEPC using the signal process characterized by the presence of a pair of muons, jets and neutrinos. In Section 2, we briefly introduce the CEPC detector design and the Monte Carlo (MC) simulation scheme. The event selection is described in Sec. 3, followed by an estimation on the precision of the signal yield in Sec. 4. Finally, conclusions are given in Sec. 5 and futher discussions are in Sec. 6.

2 Detector design and simulation samples

The CEPC will hosts two interaction points (IP) on the main ring, where the detectors at each IP should record collision data under different center of mass energies varying from $\sqrt{s} = 91.2$ GeV as a Z factory to $\sqrt{s} = 240$ GeV as a Higgs factory. To fulfill those physics programs, a baseline concept of the detector is developed based on the International Large Detector (ILD) concept [6] with further optimizations for the CEPC environment. From the most inner sub-detector component, the detector concept is composed of a silicon vertex detector, a silicon inner tracker consisting of micro strip detectors, a Time Projection Chamber (TPC), a silicon external tracker, ultra-fine segmented calorimeters, an Electromagnetic CALorimeter (ECAL) and an Hadronic CALorimeter (HCAL), a 3T superconducting solenoid, and a muon detector [4].

The CEPC simulation software package implements the baseline concept detector geometry. Events for the SM processes are generated by the Whizard [7] including the Higgs boson signal, where the detector configuration and response is handled by the GEANT4-based simulation framework, MokkaPlus [8]. Modules for digitization of the signals at each sub detector creates the hit information. Particle reconstruction has been taken place with the Arbor algorithm, which builds the reconstructed particles using calorimeter and track information[9].

The Higgs boson production and decay are simulated with the scheme, where the generated samples also contain the WW/ZZ fusion processes. All of the SM background samples, which can be classified into 2-fermion processes ($e^+e^-\to f\bar{f}$) and 4-fermion processes ($e^+e^-\to f\bar{f}f\bar{f}$), are produced as well.

3 Event Selection

Event selection is performed in several stages. The preselection builds higher-level objects, such as isolated

muons, jets, and missing momentum from the Particle Flow (PF) objects which are reconstructed by the ArborPFA. The isolation requirements on muons, identified by the PFs, are imposed. For muons with energy higher than 3 GeV, tracks inside of a cone with a half-value of opening angle θ around the candidate are examined and it is identified as an isolated muon, when a ratio between the energy of the muon candidate and a summation of the energy from all of the tracks except for the candidate in a volume defined by the cone is higher than 0.1 with $\cos\theta = 0.98$. Jets are clustered from the PFs but except for isolated lepton candidates, using the k_t algorithm for the e^+e^- collision $(ee-kt)$ with the FastJet package. Exclusive requirement ($N_{jet} = 2$) on number of jets is imposed. Events are requested to have a pair of isolated muons of positive and negative charged, and two jets successfully clustered.

The events satisfying the pre-selection criteria are separated into six categories. Depending on which physics objects ($\mu\bar{\mu}/q\bar{q}/\nu\bar{\nu}$) form the tag Z boson, the signal samples can be classified into three categories. Furthermore, distinguishing the status between having a pair of objects suppose to be decaying from the on-shell Z boson and from the off-shell Z boson where H$\rightarrow$ZZ* decay is assumed, enhances the efficiency of the event selection by applying different selection criteria for each respectively. Following notation is adopted for each category: $\mu\mu$H$\nu\nu qq$ ($\mu\mu$H$qq\nu\nu$) category is defined to be most sensitive to signal events where two characters of the top represent a pair of muons decaying from the initial Z boson, having reconstructed invariant mass $M_{\mu\mu}$ in the range 80-100 GeV with the reconstructed invariant mass of missing term $M_{\rm miss}$ due to escaping neutrinos is larger (smaller) than dijet $M_{\rm jj}$. The mass range for the other categories are chosen as 75-110 GeV for $\nu\nu$H$\mu\mu qq/\nu\nu$H$qq\mu\mu$ category and 75-105 GeV for qqH$\nu\nu\mu\mu/qq$H$\mu\mu\nu\nu$ category, taking into account the reconstructed mass resolution for this analysis. To ensure that the events are grouped into exclusive categories, further separation on recoil mass distribution of a pair of objects are applied which is described later.

On total six categories, $\mu\mu$H$\nu\nu qq$, $\mu\mu$H$qq\nu\nu$, $\nu\nu$H$\mu\mu qq$, $\nu\nu$H$qq\mu\mu$, qqH$\nu\nu\mu\mu$, qqH$\mu\mu\nu\nu$, further event selection criteria are optimised separately. Two different analysis approches are explored for this stage, the one where requirements are imposed on a set of kinematic variables (referred to "cut-based" analysis) and the one which uses a multivariate analysis technique, based on the boosted decision tree (BDT) implemented within scikit-learn package [11], in order to achieve better separation between signal and background (referred to "BDT" analysis).

For the cut-based analysis, the signal to background ratio is minimized by the following requirements. The invariant mass $M_{\mu\mu}$ of the two muons, the invariant mass $M_{\rm jj}$ of two jets and the missing mass $M_{\rm miss}$ are required to fall into the mass window around the Z(Z*) boson. Number of particle flow objects $N_{\rm PFO}$ in the event is required to be larger than a threshold value, which is affected and decided by the condition whether jets are originated from an on-shell Z boson or not, as well as to suppress backgrounds where the jets are reconstructed from any objects other than quark seeds coming from the Z boson. Cut on the polar angle of the sum of all visible particles $\cos\theta_{\rm vis}$ is applied to further reject background processes, such as two-fermion components which tends to be back-to-back along the beam axis. Angular differences between the reconstructed Z bosons from di-muons and di-jets $\Delta\phi_{\rm ZZ}$ is used to reduce background components as well. Kinematic properties of two on-shell Z bosons has significant overlap at $\sqrt{s} = 240$ GeV, causing overlapping of categories between interchange of on-shell Z bosons. In the two-dimensional plane of recoil mass distributions of di-objects, two exclusive regions are defined and are used to confine the category to ensure that the events are grouped into mutually exclusive categories. For example, in the $M^{\rm recoil}_{\mu\mu}$-$M^{\rm recoil}_{\rm jj}$ plane, a region covering majority of Z($\rightarrow q\bar{q}$)H($\rightarrow$ZZ*$\rightarrow\mu\mu\nu\bar{\nu}$) signal can be defined as

$$M^{\rm recoil}_{\mu\mu} - M_{\rm H} > \left|M^{\rm recoil}_{\rm jj} - M_{\rm H}\right| \quad (for M^{\rm recoil}_{\mu\mu} > M_{\rm H})$$
$$< -\left|M^{\rm recoil}_{\rm jj} - M_{\rm H}\right| \quad (for M^{\rm recoil}_{\mu\mu} < M_{\rm H})$$

where $M_{\rm H}$ represents the Higgs boson mass of 125 GeV. A requirement, denoted by "*not-qqHZZ*", has been added to the cut sequence for $\mu\mu$H$qq\nu\nu$ category where events are rejected if reconstructed recoil masses are included in above region. Similarly, two kinds of "*not-xxHZZ*" (xx : $\mu\mu$ or $\nu\nu$ or qq) are included in the selection for each category. Table 1 summaries the selection criteria applied across all the categories considered.

The signal and background reduction efficiencies as well as expected number of events running at $\sqrt{s} = 240$ GeV with an integrated luminosities of 5.6 ab^{-1} after the event selection are listed in the Table 2. Most sensitive signal channel and a sub-leading signal channel which is the production process by replacing the decays of on-shell Z bosons, per category is separately shown for the signal component. In general, the analysis achieves a strong background rejection, while the signal selection efficiencies of approximately 30% and higher are kept. The main background which is common in all categories is the other Higgs decays. Four fermion processes, such as $e^+e^-\rightarrow$ZZ $\rightarrow\mu\mu qq$ and $e^+e^-\rightarrow$ZZ $\rightarrow\tau\tau qq$ due to the similarity of kinematics, have large

Table 1 Overview of the requirements applied when selecting events (cut-based).

Pre-selections						
$N(l) = 2$, where leptons(l) should pass the isolation criteria $N(\mu^+) = 1$, $N(\mu^-) = 1$ with $E(\mu^\pm) > 3$ GeV $N(jet) = 2$						
Selection (Cut-based)	$\mu\mu$H$\nu\nu qq$	$\mu\mu$H$qq\nu\nu$	$\nu\nu$H$\mu\mu qq$	$\nu\nu$H$qq\mu\mu$	qqH$\nu\nu\mu\mu$	qqH$\mu\mu\nu\nu$
Mass order	$M_{\text{miss}} > M_{\text{jj}}$	$M_{\text{miss}} < M_{\text{jj}}$	$M_{\mu\mu} > M_{\text{jj}}$	$M_{\mu\mu} < M_{\text{jj}}$	$M_{\text{miss}} > M_{\mu\mu}$	$M_{\text{miss}} < M_{\mu\mu}$
$M_{\mu\mu}$ (GeV)	[80, 100]		[60, 100]	[10, 60]	[15, 55]	[75, 100]
M_{jj} (GeV)	[15, 60]	[60, 105]	[10, 55]	[60, 100]	[75, 105]	
M_{miss} (GeV)	[75, 105]	[10, 55]	[75, 110]		[70, 110]	[10, 50]
$M_{\mu\mu}^{\text{recoil}}$ (GeV)	[110, 140]		-	-	[175, 215]	[115, 155]
M_{vis} (GeV)	-	[175, 215]	[110, 140]		[115, 155]	[185, 215]
$M_{\text{jj}}^{\text{recoil}}$ (GeV)	[185, 220]	-	-	-	[110, 140]	
N_{PFO}	[20, 90]	[30, 100]	[20, 60]	[30, 100]	[40, 95]	[40, 95]
$\lvert\cos\theta_{\text{vis}}\rvert$	< 0.95					
$\Delta\phi_{\text{ZZ}}$ (degree)	[60, 170]	[60, 170]	< 135	< 135	-	[120, 170]
Region masking	*not-*$\nu\nu HZZ$ & *not-*$qqHZZ$		*not-*$\mu\mu HZZ$ & *not-*$qqHZZ$		*not-*$\nu\nu HZZ$ & *not-*$\mu\mu HZZ$	

contributions in the $\mu\mu$H$qq\nu\nu/qq$H$\mu\mu\nu\nu$ categories and in the $\nu\nu$H$qq\mu\mu/qq$H$\nu\nu\mu\mu$ categories, respectively.

For the BDT analysis, simpler selection criteria are applied prior to the BDT discrimination. The invariant and recoil mass of the associated Z boson which is reconstructed from di-objects (i.e. a pair of muons for $\mu\mu$H$\nu\nu qq$ and $\mu\mu$H$qq\nu\nu$ categories) are required to be in the region of the signal mass window. The selection requirements on the number of particle flow objects and the polar angle of the sum of all visible particles are also applied as used in the cut-based analysis.

A boosted decision tree is then trained on remaining signal and background events for each category separately. The boosting algorithm utilized in this analysis is the AdaBoost scheme [12]. The input variables to the BDT are defined as follows:

- $M_{\mu\mu}$, M_{jj}, M_{miss} : invariant mass of di-objects
- N_{PFO} : number of PFOs
- $\cos\theta_{\text{vis}}$: polar angle of the sum of all visible particles
- $\Delta\phi_{\text{ZZ}}$: angle between a Z boson reconstructed from the two muons and that reconstructed from the two jets
- $M_{\text{jj}}^{\text{recoil}}$, M_{vis} : recoil mass of the di-jets and invariant mass of all particles (for $\mu\mu$H$\nu\nu qq/\mu\mu$H$qq\nu\nu$ categories)
- $M_{\text{jj}}^{\text{recoil}}$, $M_{\mu\mu}^{\text{recoil}}$: recoil mass of the di-jets and the di-muons (for $\nu\nu$H$\mu\mu qq/\nu\nu$H$qq\mu\mu$ categories)
- $M_{\mu\mu}^{\text{recoil}}$, M_{vis} : recoil mass of the di-muons and invariant mass of all particles (for qqH$\nu\nu\mu\mu/qq$H$\mu\mu\nu\nu$ categories)
- P_{vis}, $P_{t,\text{vis}}$: magnitude of the momentum and transeverse momentum from summation of all visible particles
- $E_{\text{j}}^{leading}$, $E_{\text{j}}^{sub.}$: energy of the leading jet and the sub-leading jet
- $P_{t,\text{j}}^{leading}$, $P_{t,\text{j}}^{sub.}$: magnitude of transeverse momentum of the leading jet and the sub-leading jet

The BDT analysis exploits the increased sensitivity by combining the 14 input variables into the final BDT discriminant. Fig. 2 shows the obtained BDT score distributions for signal and background samples. For the final separation of signal and background events, the cut value on the BDT score is chosen so as to maximize a significance measure $S/\sqrt{S+B}$, where for a chosen cut, S(B) is the number of signal(background) events above this cut. The cut values as well as the other selection criteria are summrized in Table 3.

4 Result

An unbinned maximum likelihood fit is performed to extract the signal yield for each of six categories. The obtained signal and background distributions of recoil mass spectrum M_{Z}^{recoil} against the initial Z boson in the range 110-140 GeV, are added to make up a pseudo-experimental result, while the likelihood template is constructed from sum of the Probability Density Function (PDF) describing the distributions of M_{Z}^{recoil} for the signal and the background individually. The normalized distribution of M_{Z}^{recoil} for signal events is described by sum of a double sided Crystall Ball function and small Gaussian tails for $\mu\mu$H$\nu\nu qq$ ($\mu\mu$H$qq\nu\nu$) categories and a Breit-Wigner function convolved with a Gaussian for the rest of four signal categories. For the SM background components, a continuous PDF is constructed using the kernel density estimation technique [13] for each component. The background events from the other Higgs decay channels are modeled by the same PDF as the signal in each category, except for the channels having small number of events (< 20) where

Table 2 Summary of the selection efficiency ϵ and the number of expected events $N_{evt.}$ for each category after the final event selection.

(Cut-based)	$\mu\mu H\nu\nu qq$		$\mu\mu Hqq\nu\nu$		$\nu\nu H\mu\mu qq$	
Process	ϵ [%]	$N_{evt.}$	ϵ [%]	$N_{evt.}$	ϵ [%]	$N_{evt.}$
Signal ("main")	38	53	36	50	54	76
Signal ("sub")	6	8	10	14	6	9
Higgs decays Bg.	$2.2{\cdot}10^{-3}$	25	$7.0{\cdot}10^{-2}$	794	$5.3{\cdot}10^{-4}$	6
SM four-fermion Bg.	$3.7{\cdot}10^{-6}$	4	$4.9{\cdot}10^{-4}$	520	$5.6{\cdot}10^{-6}$	6
SM two-fermion Bg.	0	0	0	0	0	0
	$\nu\nu Hqq\mu\mu$		$qq H\nu\nu\mu\mu$		$qq H\mu\mu\nu\nu$	
Process	ϵ [%]	$N_{evt.}$	ϵ [%]	$N_{evt.}$	ϵ [%]	$N_{evt.}$
Signal ("main")	36	51	26	37	23	32
Signal ("sub")	8	11	7	10	4	6
Higgs decays Bg.	$1.0{\cdot}10^{-2}$	114	$2.4{\cdot}10^{-2}$	275	$1.4{\cdot}10^{-2}$	160
SM four-fermion Bg.	$4.3{\cdot}10^{-5}$	46	$1.5{\cdot}10^{-4}$	157	$1.8{\cdot}10^{-4}$	190
SM two-fermion Bg.	0	0	0	0	0	0

Table 3 Overview of the requirements applied when selecting events (BDT-based).

Pre-selections						
$N(l) = 2$, where leptons(l) should pass the isolation criteria $N(\mu^+) = 1$, $N(\mu^-) = 1$ with $E(\mu^\pm) > 3$ GeV $N(jet) = 2$						
Selection (MVA)	$\mu\mu H\nu\nu qq$	$\mu\mu Hqq\nu\nu$	$\nu\nu H\mu\mu qq$	$\nu\nu Hqq\mu\mu$	$qq H\nu\nu\mu\mu$	$qq H\mu\mu\nu\nu$
Mass order	$M_{\rm miss} > M_{\rm jj}$	$M_{\rm miss} < M_{\rm jj}$	$M_{\mu\mu} > M_{\rm jj}$	$M_{\mu\mu} < M_{\rm jj}$	$M_{\rm miss} > M_{\mu\mu}$	$M_{\rm miss} < M_{\mu\mu}$
$M_{\mu\mu}$ (GeV)	[80,100]		-	-	-	-
$M_{\rm jj}$ (GeV)	-	-	-	-	[75, 105]	
$M_{\rm miss}$ (GeV)	-	-	[75, 110]		-	-
$M_{\mu\mu}^{\rm recoil}$ (GeV)	[110, 140]		-	-	-	-
$M_{\rm vis}$ (GeV)	-	-	[110, 140]		-	-
$M_{\rm jj}^{\rm recoil}$ (GeV)	-	-	-	-	[110, 140]	
$N_{\rm PFO}$	[20, 90]	[30, 100]	[20, 60]	[30, 100]	[40, 95]	[40, 95]
$\lvert\cos\theta_{\rm vis}\rvert$	< 0.95					
Region masking	*not-$\nu\nu HZZ$ & not-$qqHZZ$*		*not-$\mu\mu HZZ$ & not-$qqHZZ$*		*not-$\nu\nu HZZ$ & not-$\mu\mu HZZ$*	
BDT score	> 0.14	> 0.01	> -0.01	> -0.01	> -0.04	> -0.01

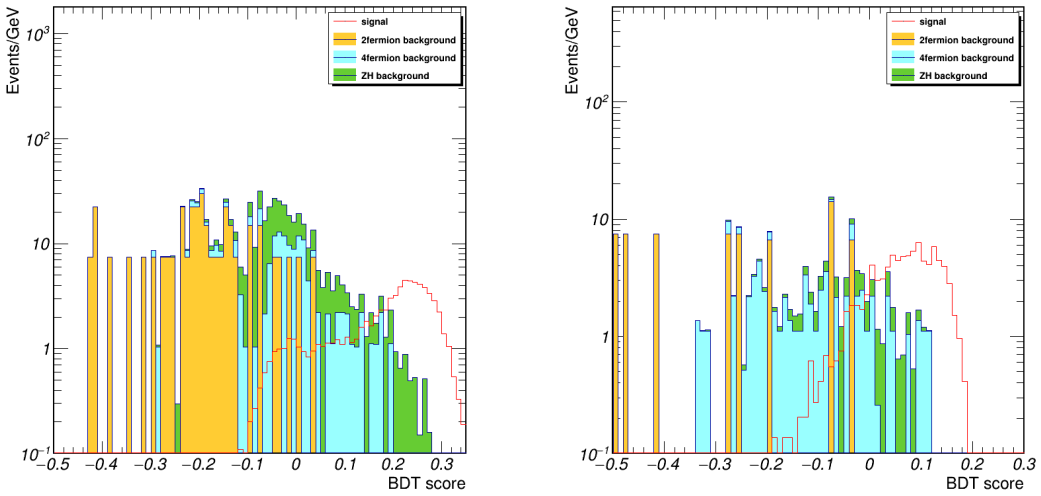

Fig. 2 (color online) BDT score distributions for two best categories: $\mu\mu H\nu\nu qq^{\rm mva}$ (left) and $\nu\nu H\mu\mu qq^{\rm mva}$ (right). The signal distribution is shown with a red histogram while background contributions, ZH (green), 4-fermion (cyan) and 2-fermion (yellow), are drawn.

a PDF from the kernel density estimation is used to describe the shape.The background components mentioned above are combined according to their fraction and are normalized to the number of events left in these categories. The template model used to the likelihood fit is then expressed as $\mu{\cdot}N_{sig}{\cdot}f_{sig} + N_{bkg}{\cdot}f_{bkg}$ where $f_{sig}(f_{bkg})$, $N_{sig}(N_{bkg})$ are the combined PDF and total number of events for signal (background) events, μ is a free parameter determined by the fit. Note that nuisance parameters, such as uncertainty of the total luminosity, are fixed to the expected values. The recoil mass distribution together with the fitting results for two of the most sensitive category is shown in Fig. 3.

The number of expected signal events can be simply represented by $N_{sig} = \mathcal{L}{\cdot}\epsilon{\cdot}\sigma_{ZH}{\cdot}\mathrm{BR(H{\to}ZZ)}{\cdot}\prod_{\mathrm{X}=\mu,\nu,q}\mathrm{BR(Z{\to}XX)}$, where $\mathcal{L}$ is the total luminosity and ϵ represents efficiencies including the detector acceptance and the analysis selection. The uncertainty of the fitting parameter μ is then regarded as the uncertainty of $\sigma_{ZH}{\cdot}\mathrm{BR(H{\to}ZZ)}$ by neglecting systematic uncertainty. Table 4 summarizes the derived relative precision on the product of the ZH cross section and the branching ratio $\Delta(\sigma{\cdot}\mathrm{BR})/(\sigma{\cdot}\mathrm{BR})$ from the cut-based analysis and the BDT analysis. The bottom row shows the combined precision that is calculated from the standard error of the weighted mean, $\sigma = 1/\sqrt{\sum_{i=1}^{n}\sigma_i^{-2}}$, where σ_i is the precision for each category. The final result for the relative statistical uncertainty of the $\sigma_{ZH}{\cdot}\mathrm{Br(H{\to}ZZ)}$ is estimated to be 8.34% in the cut-based analysis and 7.89% in the BDT analysis.

The systematic uncertainty is not taken into account in this result, since the uncertainty is expected to be dominated by the statistical uncertainty. Several sources of systematic uncertainties on Higgs measurements at the CEPC is described in Ref. [10]. Although the study in Ref. [10] has been performed with slightly different detector configuration and an operation scenario, the order of magnitude of these estimated systematic uncertainties $\mathcal{O}(0.1)\%$ on σ_{ZH}, $\mathcal{L}$ and $\mathrm{BR(Z{\to}}ff\mathrm{)}$ is also assumed for the current HZZ analysis, which are much smaller than uncertainty obtained from the fitting.

The signal yield $\sigma_{ZH}{\cdot}\mathrm{BR(H{\to}ZZ)}$ combined with independently determined σ_{ZH} allows the Higgs width Γ_{H} to be extracted as described in Sec. 1. Hence the precision of the Higgs width can be evaluated using the H→ZZ decay channel. Using the following relationship

$$\sigma_{ZH}{\cdot}\mathrm{BR(H{\to}ZZ)}{\propto}g^2_{\mathrm{HZZ}}{\cdot}\frac{\Gamma(\mathrm{H{\to}ZZ})}{\Gamma_{\mathrm{H}}}{\propto}\frac{g^4_{\mathrm{HZZ}}}{\Gamma_{\mathrm{H}}}$$

the relative uncertainty of the extracted Higgs width is obtained where the relative uncertainty on square of the coupling g^2_{HZZ} of 0.5% taken from Ref. [5] is assumed. From the cut-based analysis, the relative precision of the Higgs width $\Delta\Gamma_{\mathrm{H}}/\Gamma_{\mathrm{H}}$ is estimated to be 8.37% whereas it is 7.92% from the BDT analysis. Although the precision of H→ZZ decay measurement is to be limited by its low branching ratio, there is a room to improve from the obtained level since only small fraction of the H→ZZ decay events has been chosen and analyzed. Increasing the signal statistics under sufficient background rejection will allow further study on the precision of the signal yield

Table 4 Statistical uncertainties on the product of the ZH cross section and the branching ratio. The bottom row shows the result of combined value of the 6 categories.

Category	$\frac{\Delta(\sigma\cdot BR)}{(\sigma\cdot BR)}$ [%]	
	cut-based	BDT
$\mu\mu\mathrm{H}\nu\nu qq^{\mathrm{cut/mva}}$	15.5	13.6
$\mu\mu\mathrm{H}qq\nu\nu^{\mathrm{cut/mva}}$	48.0	42.1
$\nu\nu\mathrm{H}\mu\mu qq^{\mathrm{cut/mva}}$	11.9	12.5
$\nu\nu\mathrm{H}qq\mu\mu^{\mathrm{cut/mva}}$	23.5	20.5
$qq\mathrm{H}\nu\nu\mu\mu^{\mathrm{cut/mva}}$	45.3	37.0
$qq\mathrm{H}\mu\mu\nu\nu^{\mathrm{cut/mva}}$	52.4	44.4
Combined	8.34	7.89

5 Summary

The precision of the yield measurement $\sigma_{ZH}{\times}\mathrm{Br(H{\to}ZZ)}$ at the CEPC is evaluated using MC samples for the baseline concept running at $\sqrt{s} = 240$ GeV with an integrated luminosities of 5.6 ab^{-1}. Among the various decay modes of the H→ZZ, the signal process having two muons, two jets and missing momentum in final states has been chosen. After the event selection, relative precision is evaluated with the likelihood fitting method on signal and background. The final value combined from all of six categories is 8.34% from the cut-based analysis and 7.89% from the BDT analysis. The relative precision of the Higgs boson width, using this H→ZZ decay, is estimated by combining the obtained result with the precision of the inclusive ZH cross section and it is estimated to be 7.92% from the BDT analysis.

6 Discussion

It should be mentioned that the effective field theory (EFT) is also widely accepted as an alternative approach to explore the Higgs couplings, where additional terms for the interaction between Higgs and Z boson in the Lagrangian collapse the simple picture above [5, 14].

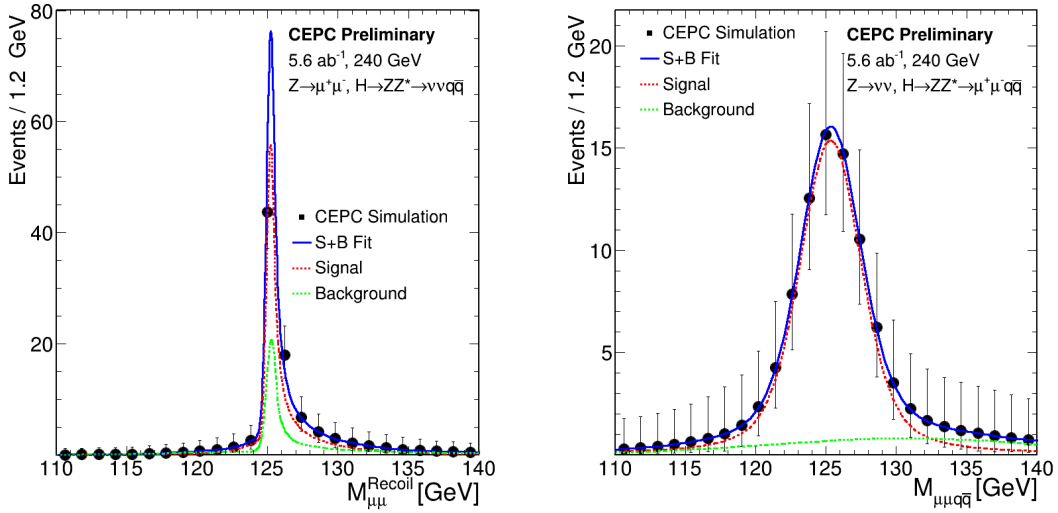

Fig. 3 (color online) Recoil mass distributions in $\mu\mu\mathrm{H}\nu\nu qq^{\mathrm{cut}}$ (left) and $\nu\nu\mathrm{H}\mu\mu qq^{\mathrm{cut}}$ (right) categories. The black dots represent the predicted results at the CEPC and the solid blue line shows the fitting curve which is broken down into signal (dashed red line) and background (dashed green line) components.

The application of EFT frameworks has been discussed on so far the production channel ($ee \to Z^* \to ZH$) for future lepton colliders [15, 16]. Higgs anomalous couplings to the Z bosons in EFT frameworks on the HZZ decay vertex can also be studied. On the other hand, Higgs CP properties and anomalous couplings to gauge bosons in the presence of BSM physics can also be measured. The fraction of the high-order CP-even contribution and the fraction of CP-odd contributions are related to SM contribution and new physics. Further study is in progress.

Acknowledgements The authors would like to thank the CEPC computing team for providing the simulation tools and samples. We also thank Yaquan Fang, Manqi Ruan, Gang Li, and Yuhang Tan for helpful discussions.

References

1. ATLAS Collaboration, G. Ada *et al.*, Observation of a new particle in the search for the Standard Model Higgs boson with the ATLAS detector at the LHC, Phys. Lett. B, **716**, 1-29 (2012), arXiv:1207.7214 [hep-ex]
2. CMS Collaboration, S. Chatrchyan *et al.*, Observation of a new boson at a mass of 125 GeV with the CMS experiment at the LHC, Phys. Lett. B, **716**, 30-61 (2012), arXiv:1207.7235 [hep-ex]
3. The CEPC Study Group, CEPC Conceptual Design Report: Volume 1 - Accelerator (2018), arXiv:1809.00285 [physics.acc-ph]
4. The CEPC Study Group, CEPC Conceptual Design Report: Volume 2 - Physics & Detector (2018), arXiv:1811.10545 [hep-ex]
5. F. An *et al.*, Precision Higgs physics at the CEPC, Chinese Physics C **43** no.4 (2019) 043002
6. T. Behnke *et al.*, The International Linear Collider Technical Design Report - Volume 4: Detectors (2013), arXiv:1306.6329 [physics.ins-det]
7. W. Kilian, T. Ohl, and J. Reuter, WHIZARD simulating multi-particle processes at LHC and ILC, Eur. Phys. J. C **71**, 1742 (2011), arXiv:0708.4233 [hep-ph]
8. P. Mora de Freitas and H. Videau, Detector simulation with MOKKA/GEANT4: Present and future, Presented at the International Workshop on Linear Colliders (LCWS 2002), 623-627 (2002), https://inspirehep.net/literature/609687
9. M. Ruan *et al.*, Reconstruction of physics objects at the Circular Electron Positron Colluder with Arbor, Eur. Phys. J. C **78** 426 (2018)
10. Z. Chen *et al.*, Cross section and Higgs mass measurement with Higgsstrahlung at the CEPC, Chinese Physics C **41** no.2 (2017) 023003
11. Pedregosa *et al.*, Scikit-learn: Machine Learning in Python, JMLR 12, pp. 2825-2830, (2011)
12. Y. Freund, and R. Schapire, A Decision-Theoretic Generalization of On-Line Learning and an Application to Boosting, Journal of Computer and System Sciencesss, **55**, 119-139, (1997)
13. K. Cranmer, Kernel estimation in high-energy physics, Comput. Phys. Commun. **136** , 198-207, (2001)
14. T. Barklow *et al.*, Improved formalism for precision Higgs coupling fits, Phys. Rev. D **97** (2018) 053003
15. I. Anderson, *et al.*, Constraining anomalous HVV interactions at proton and lepton colliders, Phys. Rev. D, **89**, (2014) 035007
16. N. Craig, *et al.*, Beyond Higgs couplings: probing the Higgs with angular observables at future e+e- colliders, JHEP 03 (2016) 050